1238 J. Med. Chem. 2010, 53, 1238–1249
DOI: 10.1021/jm901525b

Journal of Medicinal Chemistry Article

Novel Synthesis and Structural Characterization of a High-Affinity Paramagnetic Kinase Probe for the Identification of Non-ATP Site Binders by Nuclear Magnetic Resonance

Franklin J. Moy,[†] Arthur Lee,[‡] Lori Krim Gavrin,[‡] Zhang Bao Xu,[†] Annette Sievers,[†] Elizabeth Kieras,[†] Wayne Stochaj,[†] Lidia Mosyak,[†] John McKew,[‡] and Désirée H. H. Tsao*,[†]

[†]*Structural Biology and Computational Chemistry and* [‡]*Chemical Sciences, Wyeth Research, 200 CambridgePark Drive, Cambridge, Massachusetts 02140*

Received October 14, 2009

To aid in the pursuit of selective kinase inhibitors, we have developed a unique ATP site binder tool for the detection of binders outside the ATP site by nuclear magnetic resonance (NMR). We report here the novel synthesis that led to this paramagnetic spin-labeled pyrazolopyrimidine probe (**1**), which exhibits nanomolar inhibitory activity against multiple kinases. We demonstrate the application of this probe by performing NMR binding experiments with Lck and Src kinases and utilize it to detect the binding of two compounds proximal to the ATP site. The complex structure of the probe with Lck is also presented, revealing how the probe fits in the ATP site and the specific interactions it has with the protein. We believe that this spin-labeled probe is a valuable tool that holds broad applicability in a screen for non-ATP site binders.

Introduction

Kinases belong to a large family of proteins known to regulate many cellular processes that are implicated in pathologies encompassing cancer and autoimmune, metabolic, inflammatory, neurological, and infectious diseases. They play important roles in signal transduction and coordination of complex cell cycle function and apoptosis, transferring a phosphate group from ATP to the hydroxyl group of a substrate, which includes, but is not limited to, serine, threonine, or tyrosine residues. Thus, regulation of kinase activity has the potential to treat many disorders. A large number of kinase inhibitor programs are currently active in the pharmaceutical industry, targeting a wide range of the more than 500 known human kinases. To date, this effort has led to 11 approved kinase inhibitors that target the highly conserved ATP site for oncology indications.[1,2] Additionally, many kinase inhibitors are in clinical trials, including the first non-oncology kinase inhibitor, targeting Jak-3, 3-{4-methyl-3-[methyl-(7*H*-pyrrolo[2,3-*d*]pyrimidin-4-yl)amino]piperidin-1-yl}-3-oxopropionitrile, CP-690550,[3] which is currently in phase II/III.

The catalytic domain of kinases shows a high degree of sequence homology, especially for kinases that belong to the same family. They share a common ATP binding site with a conserved activation loop and similar three-dimensional structure.[4] Consequently, a major challenge in kinase research exists in achieving selectivity among the >500 family members, since they all process the same substrate. In addition to requiring selectivity against other kinases and ATP-binding proteins, these ATP site inhibitors must also bind tightly to overcome the high physiological concentration of ATP in the cell. Currently, the development of novel ATP site inhibitors is also becoming increasingly challenging, as many ATP competitive scaffolds have been disclosed. To develop compounds with better selectivity among kinases, inhibitors that bind outside the ATP site show great promise and are currently being explored by many groups. Inhibitors that can target kinases in sites nearby the substrate binding locations have the potential to exploit the features that are unique to each kinase. For example, 4-[(4-methylpiperazin-1-yl)-methyl]-*N*-{4-methyl-3-[(4-pyridin-3-ylpyrimidin-2-yl)amino]-phenyl}benzamide, also known as Imatinib, binds to Abl, a platelet-derived growth factor receptor and stem cell factor receptor, and has been used to successfully treat cancer.[5,6] This drug binds in the substrate pocket and further extends into the ATP site.[2] Structural work further reveals that it stabilizes an inactive conformation of Abl kinase,[7] and this binding mode has been observed in other known kinase inhibitors, such as 4-{4-[3-(4-chloro-3-trifluoromethylphenyl)ureido]phenoxy}pyridine-2-carboxylic acid methylamide (Sorafenib, BAY-439006) binding to B-Raf[8] and 1-(5-*tert*-butyl-2-*p*-tolyl-2*H*-pyrazol-3-yl)-3-[4-(2-morpholin-4-ylethoxy)naphthalen-1-yl]urea (BIRB796) to p38.[9] These inhibitors are called type II, as they move the activation loop (DFG loop) to an "out" conformation, creating a pocket next to the ATP site. Type I inhibitors, on the other hand, bind in the ATP site with the DFG loop in the "in" conformation. Occupation of the pocket next to ATP induced by type II inhibitors provides another possibility for kinase selectivity, as this region is much less conserved than the ATP binding region. The success of type II inhibitors has broadened the kinase inhibitor field tremendously. Non-ATP site (NAS)[a]

*To whom correspondence should be addressed: 200 CambridgePark Dr., Cambridge, MA 02140. Phone: (617) 665-5667. Fax: (617) 665-5682. E-mail: dtsao@wyeth.com.

[a] Abbreviations: Abl, Abelson tyrosine kinase; AMP-PNP, adenylyl-imidodiphosphate; B-Raf, V-raf murine sarcoma viral oncogene homologue B1; Jnk, C-Jun protein kinase; Jak-3, Janus kinase 3; LANCE, homogeneous time-resolved fluorescence quenching assay; Lck, lymphocyte-specific protein tyrosine kinase; KD, kinase domain; Mek-1, meiosis-specific serine/threonine protein kinase; NAS, non-ATP site; PRE, paramagnetic relaxation enhancement; TEMPO, 2,2,6,6-tetramethylpiperidine 1-oxyl; Src, proto-oncogenic tyrosine kinase; STD, saturation transfer difference; RT, room temperature.

 Published on Web 12/28/2009

Chart 1[a]

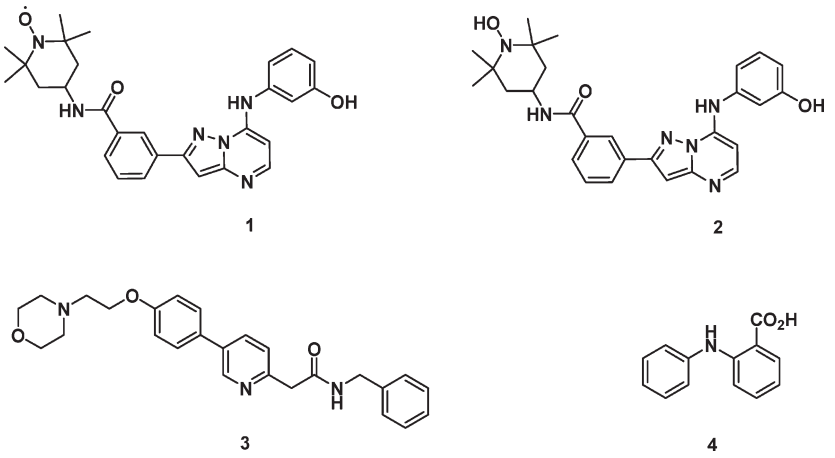

[a] **1**: Paramagnetic kinase inhibitor probe; **2**: **1** in reduced state; **3**: KX-01; **4**: *N*-phenylanthranilic acid.

binders have the potential to be exploited in conjunction with common ATP binding motifs to create more potent and selective drugs.

We present here the design, synthesis, application, and potential implications of a nanomolar-affinity, paramagnetic kinase inhibitor [**1**, reduced form, **2** (Chart 1)] as a tool to aid in the discovery of new NAS binders using nuclear magnetic resonance (NMR) spectroscopy. NMR is a well-known technique used to characterize intermolecular interactions and has been widely used in the drug discovery process for finding hits, validating leads, and subsequent optimization.[10] An attractive feature of NMR is that it is a sensitive method that can detect weak interactions up to the millimolar range.[11] It is a method uniquely suited to screening and detecting NAS binders, where the main site of a target is occupied by a ligand during a screen.[12] NAS binders have been identified using paramagnetic probes, such as organic nitroxide radicals coupled to known ATP site binders.[10,13−15] Groups such as 2,2,6,6-tetramethylpiperidine-1-oxyl (TEMPO) radicals are widely used as spin probes due to their electron paramagnetic resonance, slow electronic relaxation time, and prolonged radical stablility.[16] The unpaired electron exerts a dramatic relaxation effect on the neighboring protons as the electron has a much higher gyromagnetic ratio (658 times) compared to that of a proton,[17] the effects of which are easily detected by NMR relaxation experiments. Protons from the protein and ligands that are within 15−25 Å of the paramagnetic center are broadened, and their signals are easily detected in an NMR experiment.

Previously reported work[13] of McCoy et al. describes MnATP as a probe, where Mn^{2+} was chelated to ATP and this complex is then used to detect binding of a diphenylamine inhibitor with Mek-1 kinase. This probe can be applied to nucleotide binding proteins in general and therefore provides a versatile and especially useful way to find NAS binders to kinases. However, this probe binds weakly to most proteins and, as a result, requires an excess to ensure full binding occupancy. Jahnke and co-workers have also used spin-labeled ligands as a screening tool for several biological systems,[14,15,17] including a spin-labeled adenine analogue with TEMPO, developed for screening NAS inhibitors of kinases. More recently, an indazole analogue containing TEMPO was synthesized as a probe for NAS screening against Jnk.[18] Although these probes are efficient in detecting nearby

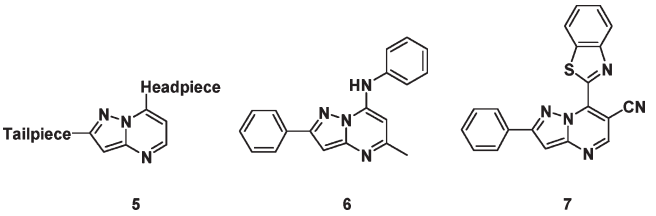

Figure 1

binders, they bind to their kinase targets with relatively low affinity and have not been broadly profiled. For weak binding probes, additional control experiments are necessary to validate that the probe binds exclusively at the ATP-binding site. If nonspecific binding is observed, false positive results will be obtained.

Here, we discuss the advantages and utility of our low-nanomolar affinity TEMPO-containing probe **1** and its application to the kinase domains (KDs) of Lck and Src kinases by NMR to identify NAS binders. Using **1**, we confirmed the binding of a known non-ATP competitive selective Src binder, *N*-benzyl-2-{5-[4-(2-morpholin-4-ylethoxy)phenyl]pyridin-2-yl}acetamide, also known as KX-01[19−21] (**3**, Chart 1), and also established that *N*-phenylanthranilic acid (**4**, Chart 1) binds proximal to the ATP site in Lck. In addition, we present a novel synthetic route used to obtain the previously unreported 3-bromo-1*H*-pyrazol-5-amine (**17**). This useful intermediate (**17**) was central in the synthesis of **1**. We will discuss the synthesis, features, and applications of **1**. Probe **1** has the potential to be used as a screening tool for a variety of kinases in the identification of NAS binders by NMR. Lastly, the crystal structure of **1** with Lck KD will also be presented, revealing how the probe is oriented in the ATP binding site of Lck and the specific interactions it makes with the protein.

Results and Discussion

Rationale for the Design and Synthesis of the Paramagnetic Probe. Despite the initial success in previously synthesized paramagnetic probes, it would be of clear interest to obtain an ATP competitive probe with higher affinity for a broad range of kinases, which could be used as a screening tool for NAS binders. Our efforts have identified the pyrazolo[1,5-α]pyrimidine core (**5**, Figure 1) as a kinase inhibitor. Via modification of the head- and/or tailpiece, high affinity was

achieved against multiple kinases. Our efforts to prepare the spin-labeled probe required a flexible synthesis of these types of molecules. Syntheses of pyrazolo[1,5-α]pyrimidines with aryl substitution at the "tailpiece" and aniline or aryl substitution at the "headpiece" of the molecule, such as compounds **6**[22] and **7**,[23] have been previously conducted, as shown in Figure 1.

Previous efforts in our laboratory have shown that cyclization of various aminopyrazoles with the sodium salt of ethyl formylacetate provides the pyrazolo[1,5-α]pyrimidine core, **5**.[24] In addition, our work also showed that these cores could be synthesized starting from more readily available reagents such as α-bromoketones.[24] Displacement of the α-bromo group with cyanide followed by condensation with hydrazine afforded pyrazole **9**. Cyclization with diethylethoxymethylene malonate and subsequent saponification/decarboxylation yielded the pyrazolo[1,5-α]pyrimidin-7-one, **10**, in five steps and in 32% overall yield (Scheme 1).

Standard chemistry[25] would allow for elaboration on the pyrimidone core, as shown in Scheme 2, to afford a variety of compounds with diverse aniline headpieces but with limited diversity in the tail region, **13** (Scheme 2).

In our quest to synthesize the best probe for NMR studies, we examined a collection of uniquely substituted pyrazolopyrimidines. However, the substitution of the tailpiece moiety was limited to accessible aminopyrazoles. Ideally, the starting point would be 3-bromo-1*H*-pyrazol-5-amine that has a handle for diverse functionalization. Despite many recent developments in aminopyrazole chemistry,[26] this compound has not been reported. Therefore, our synthetic efforts became focused on synthesizing this key intermediate whereby a convergent and flexible synthesis allowing for late stage diversity at both the headpiece and the tailpiece of the pyrazolo[1,5-α]pyrimidines could be achieved. These efforts resulted in the first report of the synthesis of 3-bromo-1*H*-pyrazol-5-amine, **17**, obtained from the concomitant debromination and nitro reduction of the previously reported **16**,[27] shown in Scheme 3. The regiochemistry of the reduction product was confirmed by spectroscopic comparison of **17** with commercially available 4-bromo-1*H*-pyrazol-5-amine (Scheme 3).

Aminopyrazole, **17**, was elaborated as in the above-mentioned methodology to provide the common intermediate, **20** (Scheme 4), that is uniquely suited for rapid functionalization. From this common intermediate, synthesis of a diverse set of analogues can be realized. After amine installation in the headpiece region, assorted tailpiece moieties may be installed using Buchwald, Heck, Sonogashira, or Suzuki couplings. Since the tailpiece is built in at a late stage of the synthesis, the choice of tailpiece functionality is not limited. Additionally, compared to the linear route shown in Schemes 1 and 2, a route involving intermediate **20** enables

Scheme 1[a]

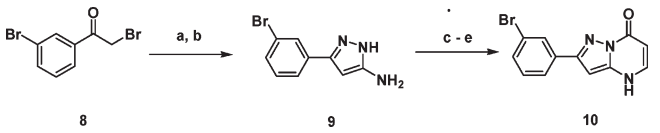

8 9 10

[a] Reagents and conditions: (a) KCN, MeOH, H_2O, RT, 0.5 h, 65%; (b) hydrazine hydrate, EtOH, 100 °C, 2 h, 69%; (c) diethylethoxymethylene malonate, AcOH, reflux, 16 h, 85%; (d) NaOH, EtOH, 100 °C, 3 h, 91%; (e) Dowtherm A, 250 °C, 2 h, 91%.

Scheme 2[a]

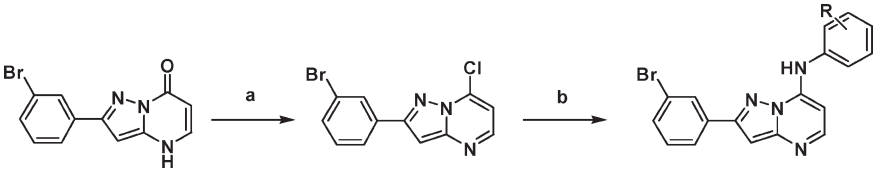

11 12 13

[a] Reagents and conditions: (a) $POCl_3$, DIPEA, 130 °C, 16 h, 83%; (b) aniline, acetic acid, dioxane, 150 °C, 10 min, microwave, 80−100%.

Scheme 3[a]

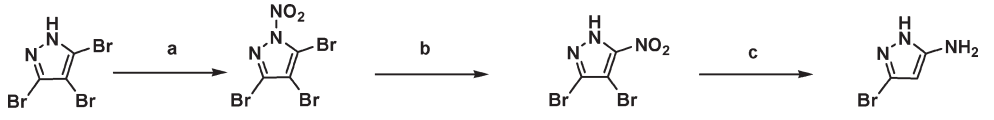

14 15 16 17

[a] Reagents and conditions: (a) nitric acid, acetic anhydride, acetic acid; (b) 3,5-dimethyl-1*H*-pyrazole, toluene, reflux, 20 min; (c) $SnCl_2 \cdot 2H_2O$, 42% over three steps.

Scheme 4[a]

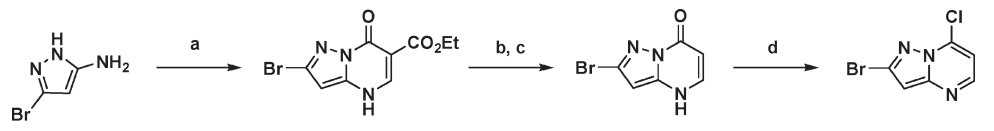

17 18 19 20

[a] Reagents and conditions: (a) diethylethoxymethylene malonate, reflux, 4 h, 77%; (b) NaOH, MeOH, H_2O, 100 °C, 2 h, 92%; (c) Dowtherm, 240 °C, 2.5 h, 98%; (d) $POCl_3$, DIPEA, 130 °C, 16 h, 77%.

Scheme 5[a]

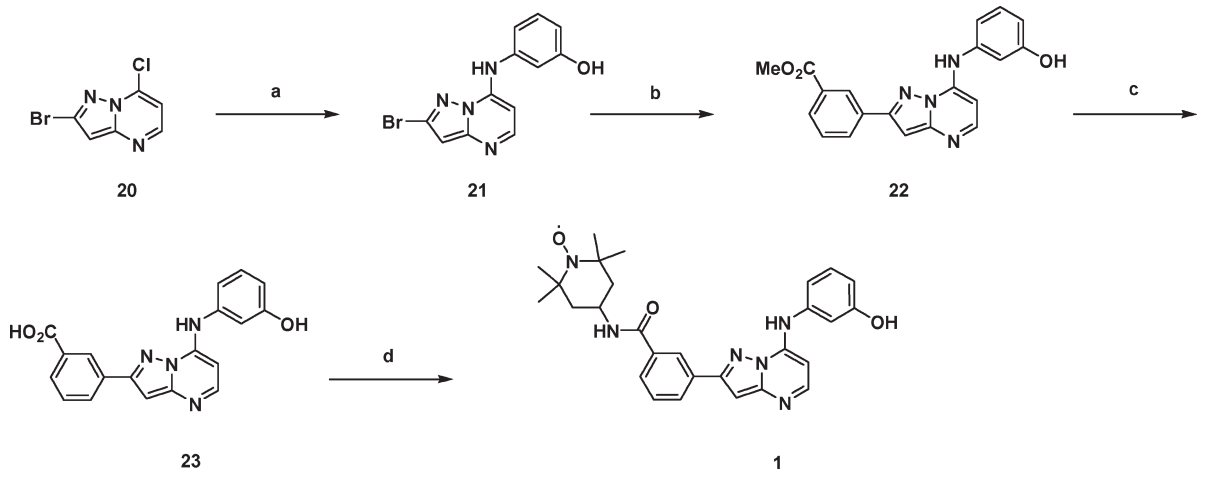

20 21 22 23 1

[a] Reagents and conditions: (a) 3-aminophenol, acetic acid, dioxane, 150 °C, 20 min, microwave, 92%; (b) 3-methoxycarbonylphenylboronic acid, $Pd(dppf)Cl_2$, 2 M K_3PO_4, dioxane, 90 °C, 1.5 h, 83%; (c) LiOH, THF, H_2O, 25 °C, 45 min, 90%; (d) 4-amino-TEMPO, BOP, Et_3N, CH_2Cl_2, 25 °C, 1.5 h, 36%.

Table 1. IC_{50} Values of **1** in Kinases from the Selectivity Panel

kinase	IC_{50} (μM)	kinase	IC_{50} (μM)
ABL1	0.005	p38alpha (MAPK14)*	> 50
Aurora B	2.9	MAPKAPK2 (MK2)	> 50
CDK1/cyclin B	> 50	PKA (PRKACA)**	> 50
CDK2/cyclin A	> 50	PKC-β (PRKCB1)	> 60
Fyn	0.005	PRKCA (PKC-α)	1.3
HCK	0.016	CSNK1G1 (CK1 γ1)	> 50
Lyn A	0.007	MAP4K2 (GCK)	0.024
SRC	0.005	PDGFRA	0.038
KDR (VEGFR2)	0.0033	RPS6KA1 (RSK1)	> 50
MAPK1 (ERK2)	> 50		

a wider array of products to be prepared due to the abundance of commercially available boronic acids.

On the basis of previously determined complex structures of various pyrazolo[1,5-α]pyrimidines with Lck (not shown), we knew that a large group such as TEMPO could be accommodated without an effect on the important interactions between the protein−ligand complex. Hence, we decided to couple 4-amino-TEMPO to a carboxylic acid. The synthesis of acid, **23**, and probe compound, **1**, from the versatile common intermediate, **20**, follows standard chemistry and is outlined below (Scheme 5).

Compound 1 Binds with High Affinity to Multiple Kinases. This compound was submitted to a Caliper kinase selectivity panel to evaluate its affinity for different kinases. Table 1 summarizes the results, showing that **1** had an IC_{50} of < 0.040 μM in eight kinases, most of them belonging to the tyrosine kinase (TK) branch of the human kinome. The IC_{50} of **1** with Lck was determined via a LANCE fluorescence assay, and it was shown to be 0.035 μM. This initial testing indicates the potential of this inhibitor to have a high affinity for many kinases, as our panel is comprised of only a small subset of kinases from the human kinome. Compound **1** was shown to be competitive with the stable ATP analogue, AMP-PNP (adenylyl imidodiphosphate), by NMR, indicating binding in the ATP binding site, subsequently confirmed by the complex structure of **1** with Lck KD presented here.

NMR Spectroscopy and Detection of NAS Binders. As reported in Table 1, our probe shows low nanomolar activity for several kinases. Several NMR experiments were conducted to evaluate **1** and its interaction with two kinases, Lck and Src kinase. Since **1** itself exhibits broad lines in the NMR spectrum, ascorbic acid was added to reduce the nitroso to the hydroxyl amine in situ (**2**, Chart 1), which resulted in sharp lines necessary for the protein titration experiment. The addition of ascorbic acid (5-fold over **1**) did not affect the binding of the test compound, as evidenced by control NMR experiments. To confirm the high affinity of **2** for Lck KD, an NMR protein titration was performed, where the line shapes of **2** in the presence and absence of the kinase were compared. The signals for **2** were monitored as Lck was added (Figure 2), and as expected for a tight inhibitor, a decrease in signal intensity with addition of Lck in a stoichiometric fashion was observed. Low nanomolar inhibitors are in slow exchange with the protein target, and the bound ligand NMR signals will broaden, since the ligand's line width is inversely proportional to its transverse relaxation rates; in this case, it becomes that of the kinase. Only the free ligand that remains in solution is observed, displaying sharp NMR signals,[28] and at equimolar amounts of **2** and Lck

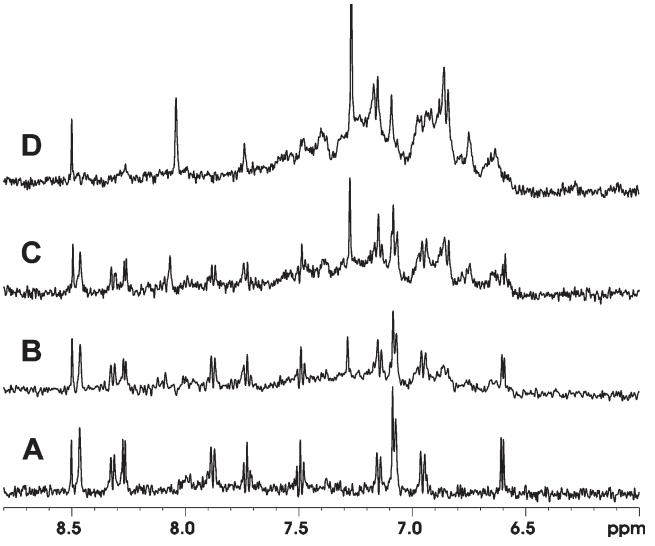

Figure 2. Titration shows **2** binds tightly to Lck KD. **2** (10 μM) with (A) 0, (B) 2.5, (C) 5, and (D) 10 μM Lck. The resonance peak at 8.51 ppm comes from the buffer.

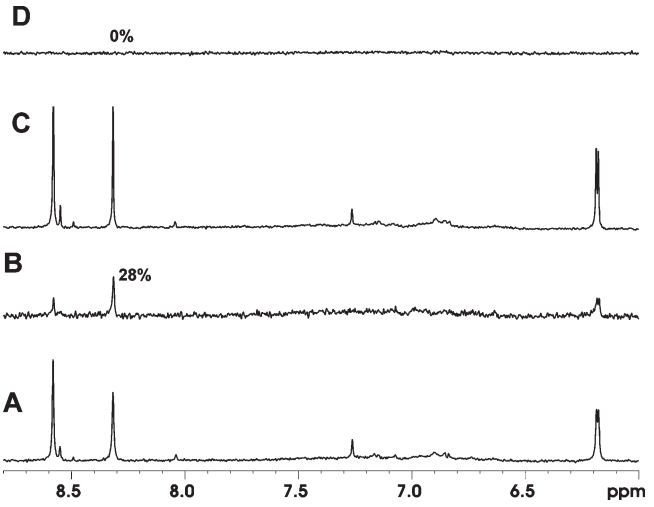

Figure 3. STD spectra of Lck and AMP-PNP in the presence and absence of **1** showing that **1** competes with AMP-PNP. (A and B) One-dimensional reference and STD spectra, respectively, of 7.5 μM Lck and 125 μM AMP-PNP. (C and D) One-dimensional reference and STD spectra, respectively, of 7.5 μM Lck, 125 μM AMP-PNP, and 10 μM **1**.

(Figure 2D), the ligand signals are no longer visible, confirming that **2**, and presumably **1**, bind with high affinity to Lck.

Binding of **1** was also monitored by the saturation transfer difference (STD) experiment with Lck. In this difference experiment, small amounts of protein are present with a large excess of ligand, the protein is saturated on and off resonance, and the saturation propagates throughout the protein via spin diffusion.[29] If the compound binds to the protein, the saturation will be transferred to the compound, which upon exchange back into solution is detected from the difference spectrum between the off and on resonance spectra. The subtracted spectrum shows only resonances that have been saturated, arising mainly from the bound compound.[29] We confirmed that **1** is an ATP site binder, by adding it as a competitor to the mixture of Lck and AMP-PNP. AMP-PNP binds to Lck, as shown in Figure 3, giving an STD signal of 28% (Figure 3B). Addition of **1** at a similar concentration to Lck completely abolishes binding of AMP-PNP, confirming that **1** binds in the ATP binding site and prevents AMP-PNP binding (Figure 3D). Similar results were also achieved with Src kinase with complete inhibition of AMP-PNP binding upon addition of **1** (spectra not shown).

The application of this paramagnetic probe was also demonstrated with the $T_{1\rho}$ experiment, in which the spin−lattice relaxation rates in the rotating frame of the ligand in the presence and absence of protein were compared.[30,31] The free ligand relaxes slowly and upon binding to the protein acquires characteristics of the large molecule and will then relax rapidly. The relaxation rate observed will be a weighted average of the relaxation rates between the free and bound states for fast exchanging systems. In the presence of a paramagnetic center, the relaxation rate of the ligand is further enhanced in the bound state due to the unpaired electron. Compound **1** enhances the relaxation of nearby protons significantly (15−25 Å radius), both for the protein and for the potential binders. Figure 4 shows the $T_{1\rho}$ control experiment with Lck and AMP-PNP. All $T_{1\rho}$ experiments were conducted with a short relaxation period of 10 ms (blue)

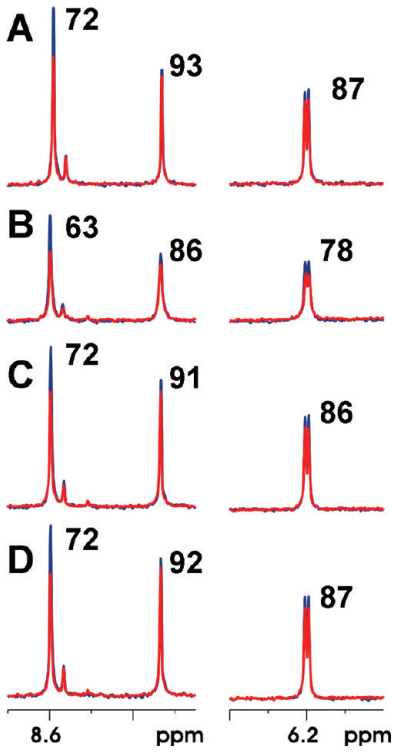

Figure 4. $T_{1\rho}$ spectra at 10 (blue) and 200 ms (red) of (A) 125 μM AMP-PNP, (B) 125 μM AMP-PNP and 7.5 μM Lck, (C) 125 μM AMP-PNP, 7.5 μM Lck, and 10 μM **1**, and (D) 125 μM AMP-PNP, 7.5 μM Lck, and 10 μM **2**. Comparison of relaxation intensity ratios of $T_{1\rho}$ spectra from panels A and B indicates that AMP-PNP binds to Lck with a reduction of 7−9% units. Relaxation intensity ratio comparison of $T_{1\rho}$ spectra between panels C and D shows no PRE of AMP-PNP. Compared to panel A, this shows that AMP-PNP is free in solution.

and a long relaxation period of 200 ms (red). In the longer delay spectrum, the resonance intensity will be reduced accordingly by binding to the protein and/or enhancement by **1**. The effects of the test compound binding and paramagnetic relaxation enhancement (PRE) are evaluated in two ways: (1) by measuring the changes in the relaxation intensity ratio of the $T_{1\rho}$ spectra acquired at 10 ms versus 200 ms delays (i.e., comparing red and blue traces in Figure 4) and (2) by noting changes in spectra acquired at 200 ms delays (i.e., comparing red and red traces in panels A and B and panels C and D of Figure 4). In Figures 4−6, the relaxation intensity ratio is reported as the percentage ratio of the peak at 200 ms to the peak intensity at 10 ms. Panels A and B of Figure 4 display the $T_{1\rho}$ spectra obtained for AMP-PNP and AMP-PNP with Lck, respectively. As anticipated, a decrease in the magnitude of the AMP-PNP signal at both 10 and 200 ms is observed in Figure 4B (relative to free AMP-PNP) due to binding to Lck. Upon addition of **1** and its reduced form, **2** (panels C and D of Figure 4, respectively), there is a significant increase in the ratios (panel B vs panels C and D of Figure 4), indicating that AMP-PNP no longer binds to Lck and is competed off by **1**. This is in complete agreement with the STD experiments presented in Figure 3. In addition, as expected, the AMP-PNP resonance relaxation intensity ratios are unchanged in Figure 4C,D.

We sought a test compound that could be used to validate **1** as a screening tool. Kinex Pharmaceuticals has reported on **3** (Chart 1), an inhibitor of Src that is not competitive with ATP and is postulated to bind to the substrate binding

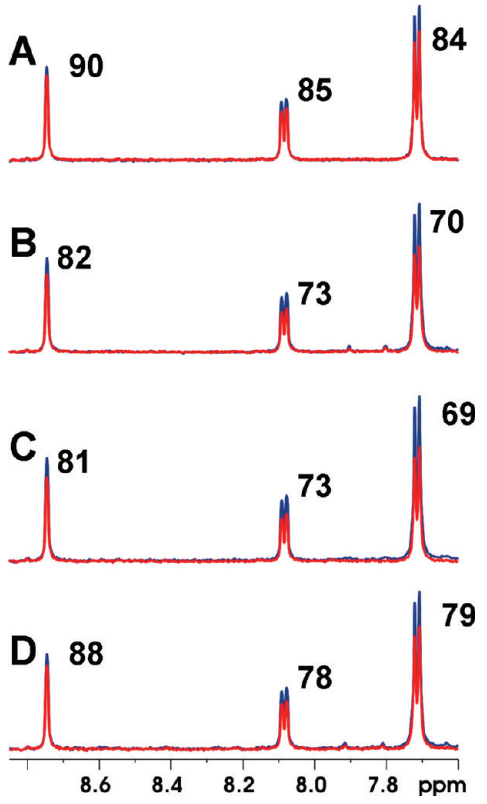

Figure 5. $T_{1\rho}$ partial aromatic spectra at 10 (blue) and 200 ms (red) of (A) 100 μM **3**, (B) 100 μM **3** and 6 μM Src, (C) 100 μM **3**, 6 μM Src, and 10 μM **1**, and (D) 100 μM **3**, 6 μM Src, and 10 μM **2**. Comparison of relaxation intensity ratios of $T_{1\rho}$ spectra of panels A and B shows that **3** binds to Src giving a 8−14% unit reduction. The 5−10% unit reduction in relaxation intensity ratios of $T_{1\rho}$ spectra of panels C and D is due to PRE.

domain.[19−21] It has been reported by Kinex that in cells **3** shows nanomolar inhibition of Src-dependent growth, whereas in assays that examine the functional activity of the Src KD, it appears to be weakly potent ($IC_{50} \sim 40$ μM).[19−21] The unique binding mode and weak affinity for the Src KD made **3** an ideal test compound for demonstrating the potential of **1** to detect NAS binders via NMR relaxation experiments. We confirmed the activity of **3** to Src KD in house ($IC_{50} >$ 20 μM) and verified that **3** binds to Src kinase by the STD experiment and did not compete with either AMP-PNP or staurosporine, a known high-affinity pan kinase inhibitor (data not shown). In addition, a titration similar to the one reported in Figure 2 was performed, and the results were in agreement with **3** binding weakly to Src KD. Figure 5 shows the $T_{1\rho}$ binding results for Src with **3**, where a decrease in peak intensity for the 200 ms delay (Figure 5A, red trace, vs Figure 5B, red trace) and a reduced relaxation intensity ratio (change of 8−14 units between panels A and B) are observed, consistent with **3** binding to Src KD. In addition, we observe PRE via a lower ratio observed in the peak at 8.74 ppm (Figure 5C) compared to that in Figure 5D, indicating that **3** and **1** are binding simultaneously to Src.

The utility of **1** was also demonstrated in the characterization of **4** (Chart 1) binding to Lck. Compound **4** was chosen to be tested as a potential binder since it is a common scaffold in known drugs[32] and, due to its simple core, would likely be a weak binder. We verified that **4** binds to Lck KD by the STD experiment, and it did not compete with staurosporine (spectra not shown). Figure 6 displays the $T_{1\rho}$ experiments

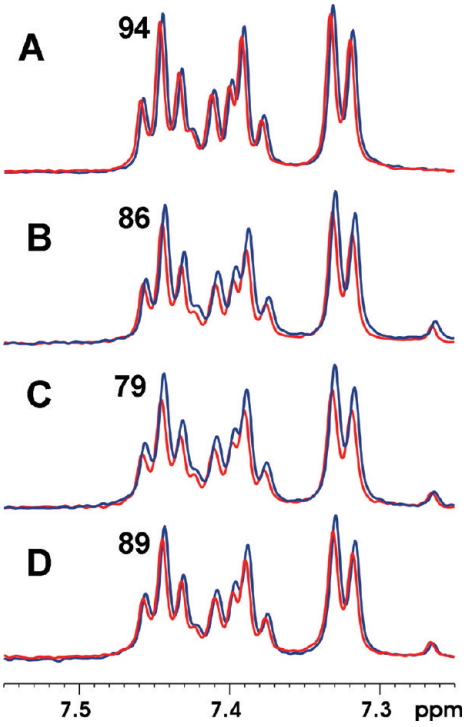

Figure 6. $T_{1\rho}$ partial aromatic spectra at 10 (blue) and 200 ms (red) of (A) 100 μM **4**, (B) 100 μM **4** and 7.5 μM Lck, (C) 100 μM **4**, 7.5 μM Lck, and 10 μM **1**, and (D) 100 μM **4**, 7.5 μM Lck, and 10 μM **2**. Comparison of relaxation intensity ratios of $T_{1\rho}$ spectra of panels A and B shows that **4** binds to Lck giving an 8% unit reduction. The 10% unit reduction in relaxation intensity ratios of $T_{1\rho}$ spectra of panels C and D is due to PRE.

performed, which provides evidence that **4** binds in a site adjacent to the ATP site. Panels A and B of Figure 6 confirm the binding of **4** to Lck. Upon addition of **1**, there is a reduction in the relaxation intensity ratio (Figure 6C,D), similar to the results obtained for **3** and Src with **1**, showing simultaneous binding of **1** and **4** to Lck. In both cases, experiments displayed in Figures 5 and 6 show that the test compounds may bind differently to the kinase targets when **2** (and, by inference, **1**) is bound to the kinases. This is not unexpected, since the presence of **1** (and presumably **2**) keeps the kinase in a closed conformation. Control experiments conducted with all three test compounds (**3**, **4**, and AMP-PNP) and **1** show that their relaxation rate did not change significantly in the absence of protein.

Structure of 1 with Lck. The ribbon diagram of Lck and positioning of **1** in the ATP-binding site are shown in Figure 7. The diagram is oriented such that the TEMPO moiety points toward the bulk solvent, the phenol is buried in a deep hydrophobic pocket with the hydroxyl group hydrogen-bonded to the catalytic Lys 273, and the pyrazolopyrimidine core binds along the hinge making a hydrogen bond to the NH group of Met 319. The amide between the core and the probe tail interacts indirectly with hinge Met 319 through a water-mediated hydrogen bond. There are also a large number of van der Waals interactions with the Lck ATP-binding domain that stabilize the conformation of the bound inhibitor. Figure 7B shows these specific interactions with **1**.

The changes observed in $T_{1\rho}$ relaxation experiments for **3** and **4** are clearly due to binding to the kinases, and PRE is observed in the presence of the spin-labeled probe. The amount of PRE observed depends on factors such as the

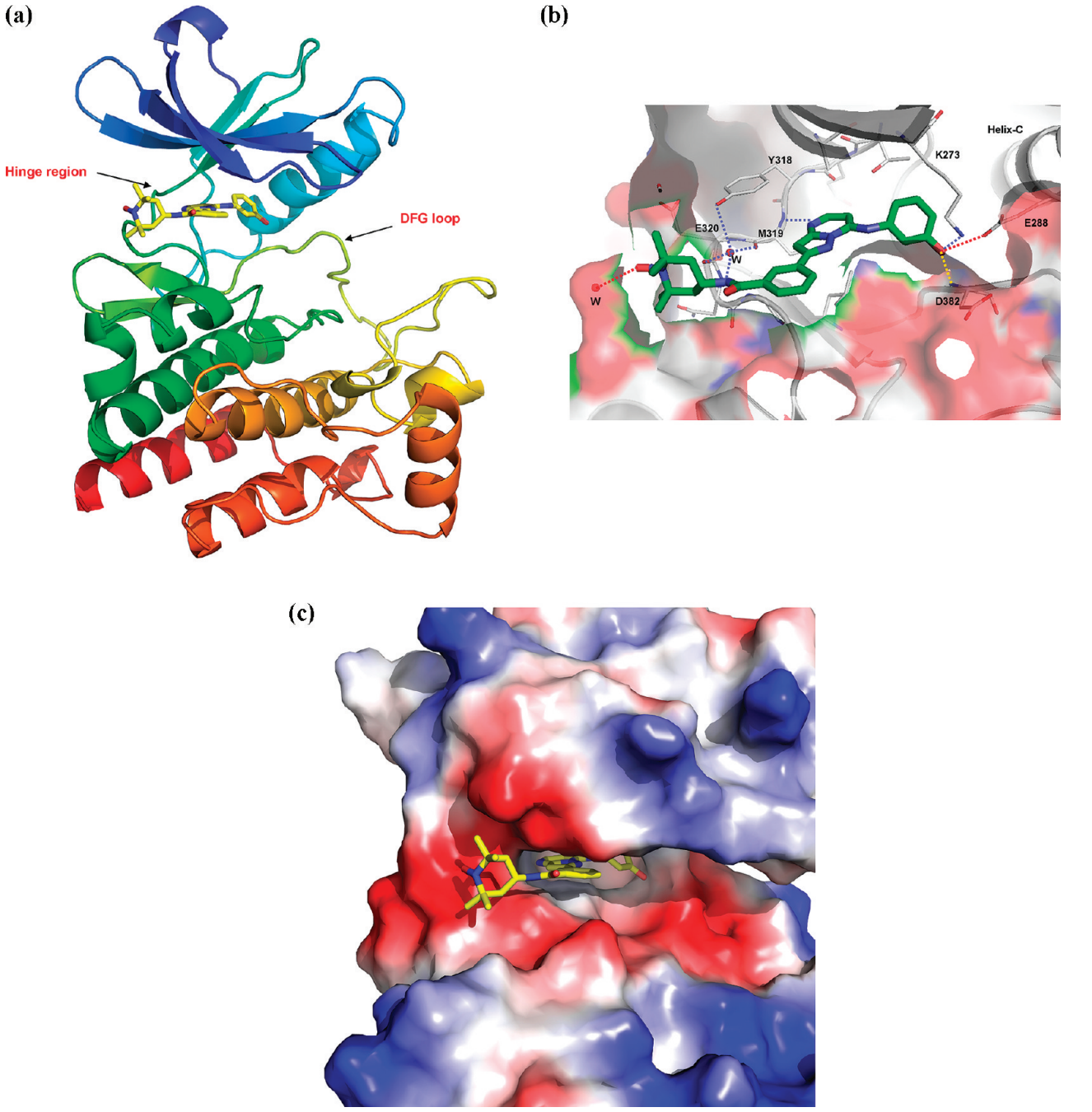

Figure 7. (A) Ribbon diagram of the catalytic domain of Lck kinase in complex with **1**. The DFG loop is in the closed ("in") conformation. **1** binds in the ATP site, and the nitroxide extends to the solvent. (B) Close-up of the complex, showing specific interactions in the complex. Several hydrogen bonds contribute to the tight binding of **1** to Lck. Lys 273 and Asp 382 make hydrogen bonds to the oxygen of the phenol moiety and Met 319, and N4 of pyrazolopyrimidine also forms a hydrogen bond. (C) Electrostatic surface area showing a 20 Å radius from the nitroxide end of **1**, colored yellow, to illustrate the range in which binders would be affected by **1**. Lck is in the closed conformation, and there is a cavity next to the probe that could potentially accommodate other binders. Blue represents positively charged residues and red negatively charged residues.

concentration of the protein, compound **1**, and the test compound, their affinities, and the distance between the test compound and the paramagnetic center. Under our experimental conditions, Lck (7.5 μM) is completely saturated with **1** (10 μM) because of its high affinity. We observe relatively weak paramagnetic effects on **4** when it is bound to Lck in the presence of **1** (Figure 6), which could be consistent with the compound being positioned far from the nitroxide end of **1** (up to 25 Å). Figure 7C shows the surface of Lck with **1** with a 20 Å radius from the nitroxide. There is a deep pocket adjacent to the ATP binding site, proximal to the peptide binding site, which could accommodate a small molecule such as **4**. The relatively weak affinity of **4** for Lck would also contribute to a weaker paramagnetic effect. Crystal structure elucidation of this ternary complex is underway to confirm the binding site of **4** relative to **1** and its specific interaction with Lck.

A comparison between the intensity ratios observed for **3** with Src in the presence of **2** (Figure 5D) and **1** (Figure 5C) shows a weak PRE. This weak effect could be explained by

the weak interaction of **3** with the KD of Src, as well as **3** possibly binding in the peptide site of Src. Compound **3** was designed to inhibit Src by binding on the peptide side, which would place it ~20−25 Å from the paramagnetic center of **1**. To obtain more specific information about the NASs, further experiments are required, such as cocrystallization of the ternary complex or competition−displacement studies. Theoretical calculations could also be performed to estimate how far the binders are from the paramagnetic center. By simulating the T_2 relaxation equation for the protein−ligand system in fast exchange, where at least 10% of the ligand is bound, we could obtain quantitative distances of up to 15 Å. This method can also detect NAS binders up to 25 Å from the paramagnetic center of **1**. However, quantitative measurement beyond 15 Å is difficult (see the Supporting Information for simulations and calculations).

Since **1** binds specifically and with high affinity to multiple kinases, it is a robust tool that can be used to screen for NAS binders. NMR is a very sensitive technique that will detect weak binders, and via adjustment of the concentration of ligand and protein used, even millimolar binders could be detected. Compound **1** has a high solubility in its reduced form in aqueous buffer of at least 50 μM, as estimated by NMR; therefore, solubility is not a limiting factor. This high level of solubility allows one to adjust the ratios of **1** to target kinases as needed. An NAS binder could be a good starting point for the development of a type II kinase inhibitor for which selectivity and potency could be further enhanced by chemically expanding the initial lead. This starting point coupled with robust high-throughput crystallography would allow for rapid structure-based optimization of these leads.

In summary, we report here a novel synthesis, characterization, and application of a low nanomolar pyrazolopyrimidine paramagnetic kinase inhibitor. This first report of 3-bromo-1*H*-pyrazole-5-amine allows access to a previously inaccessible common intermediate, **20**. This common intermediate provides entry into a wide variety of analogues where modifications can be made at either the headpiece or the tailpiece of the molecule late in the synthesis. This synthesis led to the discovery of **1**, a potent kinase inhibitor that we were able to use as a spin-labeled probe in NMR experiments. Our in-house kinase assays show that **1** binds with low nanomolar affinity to multiple kinases. We demonstrated by NMR that **1** binds to Lck and Src kinases, and it easily detects NAS binders in $T_{1\rho}$ experiments. Furthermore, we believe that high-affinity compounds such as **1** will have broad applicability when used to screen for NAS binders. These leads could be important for kinase inhibitor programs targeting NAS inhibition to achieve the goal of enhanced kinase selectivity.

Experimental Section

General Chemistry. All solvents and reagents were used as obtained. All reactions, except those involving water as a solvent, were performed under a nitrogen atmosphere. All reaction mixtures were stirred using a magnetic stir bar. All reactions were followed by thin-layer chromatography (TLC) using 250 μm prescored silica gel 60 F_{254} plates. Flash chromatography was performed using 230−400 mesh silica gel or flash columns packed with KP-SIL 60 Angstrom silica gel. Proton NMR spectra were recorded on a 400 MHz spectrometer in DMSO-d_6 solvent using TMS (δ 0.0) as a reference. High-resolution mass spectra were recorded using a Fourier transform ion cyclotron resonance (FT-ICR) mass spectrometer equipped with an actively shielded 7 T superconducting magnet and an electrospray ionization (ESI) source. Purity in two solvent systems (H_2O/CH_3CN and H_2O/MeOH) was determined using a HPLC system (Agilent) under the following conditions: UV-DAD; Agilent Zorbax SB-C18 column (3 μm, 2.1 mm × 30 mm); condition 1, solvent A (H_2O with 0.1% formic acid), solvent B (acetonitrile with 0.1% formic acid), gradient, from 95% A and 5% B to 0% A and 100% B from 0 to 7 min and to 0% A and 100% B from 7 to 9 min; condition 2, solvent A (H_2O with 0.1% formic acid), solvent B (methanol with 0.1% formic acid), gradient, from 95% A and 5% B to 0% A and 100% B from 0 to 7 min and to 0% A and 100% B from 7 to 9 min; flow rate, 0.8 mL/min; temperature, 35 °C. All compounds were determined to be >95%. ^{1}H and ^{13}C NMR tabulations as well as purity information are available in the text and Supporting Information.

3-Bromo-1*H*-pyrazol-5-amine (17). To a cooled (10 °C) solution of 3,4,5-tribromo-1*H*-pyrazole (20 g, 67 mmol) in acetic acid (300 mL) was added nitric acid (90%, 7 mL). Acetic anhydride (100 mL) was added over 20 min. After being stirred for 3 h at room temperature, the mixture was poured over ice and diluted with water. The white precipitate was washed with water and dissolved in toluene (250 mL). The organic solution was washed with water and brine, dried (Na_2SO_4), and filtered to yield a toluene solution (200 mL) of 1-nitro-3,4,5-tribromo-1*H*-pyrazole in toluene. To the toluene solution was added 3,5-dimethyl-1*H*-pyrazole (6.6 g, 67 mmol), and the mixture was heated to reflux for 20 min and cooled and the solvent removed in vacuo. The crude mixture was triturated with hexanes to give a beige solid containing 4,5-dibromo-3-nitro-1*H*-pyrazole and other products (23 g). The crude 4,5-dibromo-3-nitro-1*H*-pyrazole was reduced by refluxing with tin(II) chloride dihydrate (45 g, 200 mmol) in ethyl acetate (200 mL) and ethanol (100 mL). After 45 min, the reaction mixture was cooled and slowly poured over a vigorously stirring mixture of sodium bicarbonate (33 g, 400 mmol) in water (200 mL) and ethyl acetate (800 mL). To the resultant slurry was added Celite (30 g), and this slurry was filtered through a bed of Celite. The filter cake was washed with additional ethyl acetate (600 mL). The organic solution was washed with brine, dried (Na_2SO_4), and concentrated in vacuo. The mixture was purified on silica gel eluting with a 3% and then a 6% ethanol/dichloromethane mixture to yield a tan solid (4.42 g, 42% over three steps): ^{1}H NMR (400 MHz, DMSO-d_6) δ 11.66 (br s, 1H), 4.98−5.48 (m, 3H); ^{13}C NMR (400 MHz, DMSO-d_6) δ 149.61, 125.15, 89.15; HRMS ESI+ m/z 161.9664 [M + H].

Ethyl 2-Bromo-7-oxo-4,7-dihydropyrazolo[1,5-α]pyrimidine-6-carboxylate (18). To a solution of 3-bromo-1*H*-pyrazol-5-amine (4.14 g, 25.5 mmol) in acetic acid (150 mL) was added diethylethoxymethylene malonate (5.7 mL, 28 mmol) at room temperature. The mixture was refluxed for 4 h. The reaction mixture was then cooled to room temperature, and the acetic acid was removed in vacuo. The crude solid was suspended in cold ethanol (100 mL), filtered, and washed with cold ethanol to give 5.60 g (77%) of a pure white solid: ^{1}H NMR (400 MHz, DMSO-d_6) δ 13.25 (br s, 1H), 8.59 (s, 1H), 6.49 (s, 1H), 4.23 (q, J = 7.07 Hz, 2H), 1.28 (t, J = 7.07 Hz, 3H); HRMS ESI+ m/z 285.9822 [M + H].

2-Bromo-7-oxo-4,7-dihydropyrazolo[1,5-α]pyrimidine-6-carboxylic Acid (18b). To ethyl 2-bromo-7-oxo-4,7-dihydropyrazolo[1,5-α]pyrimidine-6-carboxylate (4.72 g, 18 mmol) in ethanol (40 mL) was added 2.5 N NaOH (20 mL) at room temperature. The reaction mixture was heated to 100 °C and stirred at this temperature for 2 h. The mixture was then cooled to room temperature and diluted with water (200 mL). Citric acid (10.5 g, 50 mmol) was added to the mixture and the mixture stirred for 45 min. The resultant solid was filtered and washed with water. The wet solid was azeotroped to dryness with toluene (200 mL) using a Dean-Stark apparatus to give 3.90 g (92%) of an off-white solid: ^{1}H NMR (400 MHz, DMSO-d_6) δ

12.98 (br s, 2H), 8.58 (s, 1H), 6.49 (s, 1H); ^{13}C NMR (400 MHz, DMSO-d_6) δ 165.25, 156.19, 147.92, 145.49, 132.98, 97.45, 95.12; HRMS ESI+ m/z 255.9367 [M − H].

2-Bromo-4,7-dihydropyrazolo[1,5-α]pyrimidin-7-one (19). A mixture of 2-bromo-7-oxo-4,7-dihydropyrazolo[1,5-α]pyrimidine-6-carboxylic acid (3.83 g, 16.4 mmol) in Dowtherm (60 mL) was heated to 240 °C for 2.5 h. At that point, the mixture was cooled to room temperature and diluted with hexanes (200 mL). The tan precipitate was filtered, resuspended and stirred in hexanes (200 mL), filtered, and washed with hexanes (200 mL) to give 3.10 g (98%) of an off-white solid. The product can be further purified by triturating in hot ethanol to yield the highly pure product (>98%): ^{1}H NMR (400 MHz, DMSO-d_6) δ 12.52 (br s, 1H), 7.87 (d, J = 7.58 Hz, 1H), 6.36 (s, 1H), 5.74 (d, J = 7.58 Hz, 1H); ^{13}C NMR (400 MHz, DMSO-d_6) δ 155.06, 142.92, 139.68, 132.00, 96.08, 91.56; HRMS ESI+ m/z 213.9612 [M + H].

2-Bromo-7-chloropyrazolo[1,5-α]pyrimidine (20). To 2-bromo-4,7-dihydropyrazolo[1,5-α]pyrimidin-7-one (3.62 g, 16.9 mmol) were added $POCl_3$ (70.0 mL) and *N*,*N*-diisopropylethylamine (6.5 mL, 37 mmol) slowly at room temperature. The reaction mixture was heated to reflux for 16 h. The mixture was cooled to room temperature, and most of the solvent was evaporated. The resultant residue was diluted with ethyl acetate (100 mL) and poured slowly into a vigorously stirring mixture of solid sodium bicarbonate (50 g), water (100 mL), and ethyl acetate (300 mL). The solution was checked for basicity (pH 8), and then the biphasic mixture was filtered through Celite. The organic layer was washed with brine (200 mL), dried (Na_2SO_4), filtered, and concentrated. The crude product was dissolved in dichloromethane (100 mL) and filtered through a silica plug with a 20% ethyl acetate/hexane mixture to remove polar impurities. Concentration followed by trituration in hexanes gave 3.01 g of a white solid (77%): ^{1}H NMR (400 MHz, DMSO-d_6) δ 8.55 (d, J = 4.55 Hz, 1H), 7.47 (d, J = 4.80 Hz, 1H), 7.14 (s, 1H); ^{13}C NMR (400 MHz, DMSO-d_6) δ 150.45, 150.07, 137.41, 134.21, 109.33, 100.29.

3-[(2-Bromopyrazolo[1,5-α]pyrimidin-7-yl)amino]-2-methylphenol (21). To 2-bromo-7-chloropyrazolo[1,5-α]pyrimidine (2.35 g, 10 mmol) and 3-aminophenol (1.15 g, 10.5 mmol) were added dioxane (20 mL) and acetic acid (0.9 mL). The reaction vessel was sealed and was heated in the microwave reactor at 150 °C for 10 min. The mixture was diluted with ethyl acetate (100 mL) and washed with concentrated aqueous sodium bicarbonate (100 mL) and then brine (100 mL), dried with Na_2SO_4, filtered, and concentrated. The resultant solid was triturated with ethanol to give 2.85 g of a tan solid after filtration and drying (92%): ^{1}H NMR (400 MHz, DMSO-d_6) δ 10.03 (s, 1H), 9.69 (s, 1H), 8.18 (d, J = 5.56 Hz, 1H), 7.24 (t, J = 7.96 Hz, 1H), 6.79−6.95 (m, 2H), 6.63−6.74 (m, 2H), 6.32 (d, J = 5.56 Hz, 1H); ^{13}C NMR (400 MHz, DMSO-d_6) δ 158.10, 150.69, 150.20, 144.82, 137.87, 132.67, 129.99, 114.72, 112.94, 111.20, 97.12, 87.85; HRMS ESI+ m/z 305.0035 [M + H].

3-{[2-(3-Methylcarboxyphenyl)pyrazolo[1,5-α]pyrimidin-7-yl]amino}phenol (22). To a solution of 3-[(2-bromopyrazolo[1,5-α]pyrimidin-7-yl)amino]phenol (0.305 g, 1 mmol) in dioxane (6 mL) were added 3-methoxycarbonylphenylboronic acid (0.271 g, 1.5 mmol) and then 2 M potassium carbonate (1.6 mL, 3.2 mmol). Nitrogen was bubbled through the solution. Pd(dppf)Cl_2 (73 mg, 0.1 mmol) was added, and then the mixture was heated at 90 °C for 1.5 h. After the mixture was cooled, it was diluted with ethyl acetate (50 mL) and shaken vigorously with brine (50 mL). The biphasic mixture was filtered through a pad of Celite; the layers were separated, and the organic layer was washed again with brine. The organic layer was dried (Na_2SO_4), filtered, and concentrated in vacuo. Eluting through a small silica plug with a 1:1 EtOAc/hexane mixture followed by trituration of the resultant solid with a 2:1 EtOAc/hexane mixture yielded 300 mg (83%) of an off-white powder: ^{1}H NMR (400 MHz, DMSO-d_6) δ 9.85 (s, 1H), 9.71 (s, 1H), 8.60−8.84 (m, 1H), 8.39 (dq, J = 1.01, 7.83 Hz, 1H), 8.19 (d, J = 5.31 Hz, 1H), 8.02 (dq, J = 0.97, 7.70 Hz, 1H), 7.50−7.77 (m, 1H), 7.28 (t, J = 7.96 Hz, 1H), 7.11 (s, 1H), 6.81−7.02 (m, 2H), 6.56−6.79 (m, 1H), 6.34 (d, J = 5.05 Hz, 1H); ^{13}C NMR (400 MHz, DMSO-d_6) δ 166.05, 158.13, 152.75, 150.52, 150.04, 145.13, 138.14, 133.33, 131.11, 130.18, 130.03, 129.31, 129.18, 126.52, 114.75, 112.84, 111.18, 92.27, 87.38, 52.19; HRMS ESI+ m/z 361.1296 [M + H].

3-{[2-(3-Carboxyphenyl)pyrazolo[1,5-α]pyrimidin-7-yl]amino}-phenol (23). To a solution of 3-{[2-(3-methoxycarbonylphenyl)-pyrazolo[1,5-α]pyrimidin-7-yl]amino}phenol (180 mg, 0.5 mmol) dissolved in THF (8 mL) was added a 1 N LiOH solution (2 mL). Additional water (6 mL) was added to make the mixture homogeneous, and then the solution was stirred for 45 min at room temperature. The reaction mixture was diluted with water (20 mL), and then formic acid (139 mg, 0.114 mL) was added. The precipitate was filtered and washed with water. The solid was triturated in ethanol and dried to yield 155 mg of a white solid (90%): ^{1}H NMR (400 MHz, DMSO-d_6) δ 13.17 (br s, 1H), 10.15 (br s, 1H), 9.77 (br s, 1H), 8.54−8.91 (m, 1H), 8.37 (dq, J = 1.01, 7.83 Hz, 1H), 8.22 (d, J = 5.56 Hz, 1H), 7.92−8.10 (m, 1H), 7.54−7.73 (m, 1H), 7.29 (t, J = 8.08 Hz, 1H), 7.13 (s, 1H), 6.83−7.01 (m, 2H), 6.73 (dd, J = 0.76, 2.27 Hz, 1H), 6.33 (d, J = 5.56 Hz, 1H); ^{13}C NMR (400 MHz, DMSO-d_6) δ 167.19, 158.26, 153.40, 149.10, 148.91, 145.85, 137.87, 132.93, 131.42, 130.88, 130.17, 129.75, 129.10, 126.94, 115.08, 113.31, 111.55, 91.76, 87.60; HRMS ESI+ m/z 347.1145 [M + H].

3-{7-[(3-Hydroxyphenyl)amino]pyrazolo[1,5-α]pyrimidin-2-yl}-*N*-(1-oxy-2,2,6,6-tetramethylpiperidin-4-yl)benzamide (1). To a solution of 3-{[2-(3-carboxyphenyl)pyrazolo[1,5-α]pyrimidin-7-yl]amino}phenol (87.0 mg, 0.25 mmol) and triethylamine (38 mg, 0.052 mL) in dichloromethane (4 mL) was added (benzotriazol-1-yloxy)tris(dimethylamino)phosphonium hexafluorophosphate (133 mg, 0.30 mmol), and the mixture was stirred at room temperature for 15 min. A solution of 4-amino-TEMPO (51 mg, 0.30 mmol) in dichloromethane (1 mL) was added. After the mixture had been stirred for 90 min, the solvent was removed. The crude material was purified on reverse phase (20 to 70% CH_3OH/H_2O) to give 44.3 mg (36%) of an off-white solid after removal of the solvent: HRMS ESI+ m/z 500.2533 [M + H]; ^{1}H NMR after treatment with 5 equiv of ascorbic acid to give **2** (400 MHz, DMSO-d_6) δ 9.77 (br s, 1H), 8.53 (s, 1H), 8.29 (d, J = 7.58 Hz, 2H), 8.13−8.23 (m, 2H), 7.86 (d, J = 8.08 Hz, 1H), 7.59 (t, J = 7.71 Hz, 1H), 7.20−7.42 (m, 2H), 7.08 (s, 1H), 6.87−6.99 (m, 2H), 6.71 (dd, J = 1.52, 8.08 Hz, 1H), 6.34 (d, J = 5.31 Hz, 1H), 4.26 (dt, J = 3.95, 8.02 Hz, 1H), 1.79 (dd, J = 3.66, 12.51 Hz, 2H), 1.56 (t, J = 12.38 Hz, 2H), 1.13 (s, 6H), 1.11 (s, 6H); ^{13}C NMR after treatment with 5 equiv of ascorbic acid to give **2** (400 MHz, DMSO-d_6) δ 165.40, 163.20, 158.15, 153.33, 150.42, 149.99, 145.01, 138.13, 135.34, 132.77, 130.04, 128.59, 128.53, 127.53, 125.07, 114.62, 112.80, 111.06, 92.20, 87.27, 58.04, 48.49, 44.66, 40.78, 32.50, 19.58.

Synthesis of Kinex Compound (3). This compound was synthesized at Wyeth according to the published procedures.[33]

Protein Expression and Purification with Lck and Src. The Lck KD construct that encodes residues Q225−P509 was expressed in insect cells using the Baculovirus expression system. This construct was designed with an N-terminal His_6 purification tag followed by a thrombin protease cleavage site (MHHHHHHSSGLVPRGS). The kinase domain was PCR amplified from a full-length Lck cDNA and subsequently cloned into pBacPAK9 (Clontech, Moutain View, CA) using Clontech's Infusion protocol. A DNA sequence-confirmed clonal isolate was recombined and transfected into insect cells with BaculoGold (BD Biosciences, San Diego, CA) following the protocol of the manufacturer. High titer virus (HTV) was prepared from pooled P^1 virus and amplified in *Spodoptera frugiperda* 9 (*Sf*9) cells at a density of 5×10^5 cells/mL and a multiplicity of infection (MOI) of 0.1 plaque forming unit (pfu)/cell. The HTV was then used to infect *S. frugiperda* 21 (*Sf*21) cells at a density of 1.9×10^6 cells/mL with an MOI of 1.5 pfu/cell. The cells were

harvested by centrifugation 72 h postinfection, resuspended in 5 mL of PBS, flash-frozen dropwise in liquid nitrogen, and then stored at −80 °C. Purification followed by lysing typically produced 100 g of cells in 800 mL of 25 mM Tris (pH 7.5), 5 mM BME, Complete Protease inhibitor Cocktail [ethylenediaminetetraacetic acid (EDTA)-free, Roche Applied Science, Indianapolis, IN], 1 mM sodium orthovanadate, 50 mM sodium fluoride, 0.25 mM AEBSF, and 5 mM β-glycerophosphate. The lysate was cleared by centrifugation and filtered through a 0.45 μm membrane. The His-tagged protein was captured on a 5 mL HisTrap HP column (GE) and eluted using a 30 to 500 mM imidazole gradient in 20 mM Tris (pH 8), 400 mM NaCl, and 5 mM 2-mercaptoethanol. The His tag was removed by thrombin cleavage during dialysis overnight against 50 mM Tris (pH 8), 20 mM NaCl, and 5 mM dithiothreitol [20 units of thrombin (Amersham)/mg of protein]. The dialyzed sample was passed through a 3 mL Poros 50 HS column. The unphosphorylated Lck protein and monophosphorylated Lck protein from the flow through were separated on a Mono Q 10/100 GL column using a NaCl gradient from 100 to 260 mM over 15 column volumes. The unphosphorylated Lck was used in the NMR experiments without further purification. The monophosphorylated Lck was concentrated using an Amicon (10000 MWCO) centrifugal concentrator and subsequently loaded onto a HiLoad 16/60 Superdex 200 column equilibrated with TBS and 5 mM DTT. The eluent which came off as a single peak was used in Lck X-ray data collection.

The human Src KD construct that encodes residues T250−L536 was expressed in *Sf*21 insect cells using the Baculovirus expression system. Src KD has a C-terminal His tag preceded by a thrombin cleavage site (LVPRGSHHHHHH) where the leucine is L536. The construct was generated by PCR amplification using full-length cDNA and cloned into pBacPAK 9 (Clontech) using Clontech's In-fusion protocol. The plasmids were transformed, and the DNA sequences of clonal isolates were confirmed. The Src KD construct was recombined and transfected into insect cells with BaculoGold (BD Biosciences) following the manufacturer's recommendations. High titer virus (HTV) was prepared from pooled P^1 virus amplified in *Sf*9 cells at a density of 5×10^5 cells/mL and an MOI of 0.1 pfu/cell. The HTV was then used to infect *Sf*21 cells at a density of 1.5×10^6 cells/mL with an MOI of 2.0 pfu/cell. The cells were harvested by centrifugation 72 h postinfection, resuspended in 5 mL of PBS-CMF/L, flash-frozen dropwise in liquid nitrogen, and stored at −80 °C. Purification of Src KD was conducted using a modification of the method of Dalgarno.[34] All procedures were performed at 4 °C. Cells from 1 L of culture were lysed in 200 mL of buffer A [25 mM Tris (pH 8), 150 mM NaCl, 10% glycerol, 5 mM imidazole, and 5 mM 2-mercaptoethanol] supplemented with 10 mM sodium fluoride, Complete Protease Inhibitor Cocktail (EDTA-free, Roche Applied Science), 25 μg/mL RNase, and 50 μg/mL DNase. Lysate was centrifuged at 25000*g* for 30 min, and the supernatant was brought to 400 mM NaCl. Lysate was subsequently batch bound to 7 mL of Ni-NTA superflow resin (Qiagen, Valencia, CA) for 1.5 h at 4 °C. The resin was packed into an Applied Biosystems column and washed with 7 column volumes of buffer A. The resin was then washed with 7 column volumes of buffer B [50 mM Tris (pH 8), 500 mM NaCl, 5% glycerol, and 1 mM DTT] supplemented with 10 mM imidazole, and then 7 column volumes of buffer B supplemented with 30 mM imidazole. The His_6-tagged Src KD was eluted with 7 column volumes of buffer B supplemented with 300 mM imidazole. The pooled peak from the Ni-NTA column was concentrated to a final volume of 5 mL using a Vivaspin 20 (10000 MWCO) centrifugal concentrator (Sartorius Biolabs, Goettingen, Germany). This concentrated sample was purified to >95% homogeneity via gel filtration at a flow rate of 1.5 mL/min on a HiLoad 1.6 × 60 Superdex 75 column (GE Healthcare, Piscataway, NJ) equilibrated with 50 mM Tris-HCl (pH 7.5), 10% glycerol, 1 mM tris(2-carboxyethyl)phosphine hydrochloride (TCEP) (Pierce Chemical Co., Rockford, IL), and 1 mM EDTA.

Enzymatic Assays: Kinase Panel. For the kinase selectivity profiling assay, all buffer salts and reagents were purchased from Sigma and were of the highest purity available. Kinases were purchased from Invitrogen and were used without further purification. Fluorescently labeled peptide substrates were purchased from Anaspec, and the peptide sequence was optimized for each kinase. Compound plates were prepared by pipetting an 11-point dose−response titration in DMSO with final assay concentrations ranging from 10 μM to 5 nM. Assay plates were prepared with a 150 nL addition of compound, followed by 7.5 μL of 50 mM assay buffer (10 mM $MgCl_2$, 0.005% Brij, and 5 mM 2-mercaptoethanol) containing substrate and ATP, followed by 7.5 μL of buffer containing enzyme. All reactions were performed at 1.5 μM peptide substrate ([S] $\ll K_m$) and at the experimentally determined K_m of ATP for each kinase. All final enzyme concentrations were below 50 nM and in most cases were ≤10 nM. The reaction mixtures were incubated at room temperature for 1−2 h depending on kinase activity but in all cases exhibited between 20 and 30% substrate phosphorylation. The reactions were quenched by the addition of 15 μL of stop buffer (100 mM HEPES, 20 mM EDTA, 0.005% Brij, and 0.2% Caliper coating reagent). Substrates and products were separated on the Caliper LC3000 instrument using standard separation protocols. The percent inhibition was calculated for each compound concentration, and the IC_{50} was determined using the following equation:

$$\%\ \text{inhibition} = \left(\max + \frac{\max - \min}{1 + \left(\frac{\text{Conc}}{IC_{50}} \right)^{\text{Hill}}} \right)$$

LANCE TR-FRET Lck. Inhibitory effects of compounds on Lck were determined using a homogeneous time-resolved fluorescence (LANCE) assay. Human full-length Lck protein was produced with a C-terminal His_6 tag using a Baculovirus expression system. The purified Lck protein was confirmed to be more than 95% pure by SDS−PAGE. Reagents are pipetted and dispensed in polystyrene V-bottom 384-well microtiter plates using Matrix PlateMate 4 × 4 liquid handling equipment. Kinase activity was determined in 20 mM HEPES buffer (pH 7.4) containing 10 mM $MgCl_2$, 1 mM 2-mercaptoethanol, 0.0025% Brij 35, 10 μg/mL BSA, 50 pM Lck, 50 μM adenosine triphosphate (ATP), and 400 nM synthetic peptide biotin-EGPWLEEEEEAYGWMDF-NH_2. The reaction mixture was incubated at room temperature for 2 h for the kinase reaction. The reactions were terminated by the addition of buffer containing 45 mM EDTA, 20 mM HEPES (pH 7.4), and 10 μg/mL BSA, containing a streptavidin-allophycocyanin (SA-APC) and a monoclonal phosphospecific antibody conjugated to a europium cryptate. The plate was incubated at room temperature for 30 min with shaking according to the manufacturer's instructions. The time-resolved fluorescence signal of SA-APC, produced only when the synthetic peptide is phosphorylated by Lck, was measured on a PerkinElmer EnVision microplate reader. Test compounds were prediluted using 100% dimethyl sulfoxide solutions to produce dose−response curves (11-point curves from final concentrations of 30 μM to ~0.5 nM). Inhibition of Lck activity with compounds of the invention was expressed as percentage inhibition of control activity exhibited in the absence of test compounds. The concentration of test compounds resulting in 50% inhibition of the Lck activity (IC_{50}) was determined from the dose−response curves.

NMR Samples and Binding Experiments. NMR samples were prepared with Lck KD at 25 mM HEPES in 200 mM NaCl, 10 mM $MgCl_2$, 1 mM DTT (pH 7.5), and a 5% DMSO/95% D_2O mixture and for Src KD at 20 mM HEPES in 200 mM NaCl, 5 mM $MgCl_2$, 2 mM DTT (pH 7.5), and a 2% DMSO/98% D_2O

mixture. Titration with the reduced probe, **2**, was performed at a compound concentration of 10 μM and with addition of Lck KD at 2.5, 5, and 10 μM. Excess ascorbic acid (5×) was added to **1** to produce its reduced form, **2**. The NMR sample used for the saturation transfer difference (STD) and $T_{1\rho}$ experiments contained 7.5 μM Lck, 125 μM AMP-PNP, and 10 μM **1**. All spectra were recorded at 25 °C with a Bruker Avance 600 MHz spectrometer equipped with a triple-resonance 5 mm inverse cryoprobe. For the STD experiments, nearly complete saturation of the protein was achieved with irradiation at 0.78 ppm for 3 s, using a train of 60 G4 Gaussian cascade shape pulses[35] of 50 ms, each separated by a 1 ms delay. Off-resonance irradiation was applied at −4 ppm, void of any protein resonances. The subtraction of STD spectra was performed internally with on- and off-resonance protein excitation using phase cycling.[36] All STD experiments were performed with 400 scans with a total time of 35 min along with a one-dimensional ^{1}H reference spectrum with 200 scans. The STD % was reported as the ratio of the peak intensities in the STD spectra and the one-dimensional ^{1}H reference spectra. $T_{1\rho}$ experiments were conducted at 10 and 200 ms spin-lock times with 128 scans. In the $T_{1\rho}$ experiments, we report the relaxation intensity ratio as a ratio of resonance signals collected with a 200 ms time over the 10 ms spin-lock spectra. A lower percentage qualitatively indicates more enhanced relaxation when comparing experiments with the probe, **1**, and with the reduced probe, **2**, for fast exchanging systems.

X-ray Crystallography. The crystals of the Lck KD−**1** complex were grown by the vapor diffusion method at room temperature. The molar ratio of the complex solution is 1:1.5 (protein:inhibitor). Equal volumes of protein complex solution [10 mg/mL protein, TBS (pH 7.5), 100 mM NaCl, and 5 mM DTT] and well solution [25% PEG 4000, 80 mM HEPES (pH 7.5), 150 mM ammonium sulfate, and 5% 2-propanol] were mixed and suspended over 1 mL of well solution. Crystals were obtained 2 days following the setup. The crystals were flash-frozen in liquid nitrogen by using a cryosolution composed of the well solution with 25% (v/v) glycerol. The 2.36 Å diffraction data were collected by using synchrotron radiation at Brookhaven National Laboratories, beamline NSLS X-29, and processed and scaled with HKL2000.[37] The crystals belong to space group $P212121$, with the following unit cell parameters: a = 42.0 Å, b = 73.8 Å, and c = 84.7 Å. The protein and inhibitor model were built using COOT[38] and refined using PHENIX[39] to a final R factor of 0.192 and an R_{free} of 0.26. The structure of Lck with **1** has been deposited in the Protein Data Bank as entry 3KXZ.

Acknowledgment. We thank Nelson Huang for providing mass spectrometry data for **1** and Karen Moreira, Shashi Mohan, Jenny Tobias, and Richard Harrison for their help in the assays of **1** with Src, Lck, and the kinase panel. We also thank Weixin Xu for input provided on X-ray crystallography.

Supporting Information Available: Purity data for all novel compounds and simulations of the T_2 relaxation equation for the protein/ligand system in fast exchange. This material is available free of charge via the Internet at http://pubs.acs.org.

References

(1) Grant, S. K. Therapeutic protein kinase inhibitors. *Cell. Mol. Life Sci.* **2009**, *66* (7), 1163–1177.
(2) Johnson, L. N. Protein kinase inhibitors: Contributions from structure to clinical compounds. *Q. Rev. Biophys.* **2009**, *42* (1), 1–40.
(3) West, K. CP-690550, a JAK3 inhibitor as an immunosuppressant for the treatment of rheumatoid arthritis, transplant rejection, psoriasis and other immune-mediated disorders. *Curr. Opin. Invest. Drugs* **2009**, *10* (5), 491–504.
(4) Noble, M. E. M.; Endicott, J. A.; Johnson, L. N. Protein kinase inhibitors: Insights into drug design from structure. *Science* **2004**, *303* (5665), 1800–1805.
(5) Druker, B. J. Imatinib as a paradigm of targeted therapies. *Adv. Cancer Res.* **2004**, *91*, 1–30.
(6) Wong, S.; Witte, O. N. The BCR-ABL story: Bench to bedside and back. *Annu. Rev. Immunol.* **2004**, *22*, 247–306.
(7) Nagar, B.; Bornmann, W. G.; Pellicena, P.; Schindler, T.; Veach, D. R.; Miller, W. T.; Clarkson, B.; Kuriyan, J. Crystal structures of the kinase domain of c-Abl in complex with the small molecule inhibitors PD173955 and Imatinib (STI-571). *Cancer Res.* **2004**, *62*, 4236–4243.
(8) Wan, P. T. C.; Garnett, M. J.; Roe, S. M.; Lee, S.; Niculescu-Duvaz, D.; Good, V. M.; Project, C. G.; Jones, C. M.; Marshall, C. J.; Springer, C. J.; Barford, D.; Marais, R. Mechanism of activation of the RAF-ERK signaling pathway by oncogenic mutations of B-RAF. *Cell* **2004**, *116* (6), 855–867.
(9) Pargellis, C.; Tong, L.; Churchill, L.; Cirillo, P. F.; Gilmore, T.; Graham, A. G.; Grob, P. M.; Hickey, E. R.; Moss, N.; Pav, S.; Regan, J. Inhibition of p38 MAP kinase by utilizing a novel allosteric binding site. *Nat. Struct. Biol.* **2002**, *9* (4), 268–272.
(10) Pellechia, M. Solution nuclear magnetic spectroscopy techniques for probing intermolecular interactions. *Chem. Biol.* **2005**, *12* (9), 961–971.
(11) Meyer, B.; Peters, T. NMR spectroscopy techniques for screening and identifying ligand binding to protein receptors. *Angew. Chem., Int. Ed.* **2003**, *42* (8), 864–890.
(12) Jahnke, W.; Florsheimer, A.; Blommers, M. J. J.; Paris, C. G.; Heim, J.; Nalin, C. M.; Perez, L. B. Second-site NMR screening and linker design. *Curr. Top. Med. Chem.* **2003**, *3* (1), 69–80.
(13) McCoy, M. A.; Senior, M. M.; Wyss, D. F. Screening of protein kinases by ATP-STD NMR spectroscopy. *J. Am. Chem. Soc.* **2005**, *127* (22), 7978–7979.
(14) Jahnke, W.; Perez, L. B.; Paris, C. G.; Strauss, A.; Fendrich, G.; Nalin, C. M. Second-site NMR screening with a spin-labeled first ligand. *J. Am. Chem. Soc.* **2000**, *122* (30), 7394–7395.
(15) Jahnke, W.; Ruedisser, S.; Zurini, M. Spin label enhanced NMR screening. *J. Am. Chem. Soc.* **2001**, *123* (13), 3149–3150.
(16) Deschamps, M. L.; Pilka, E. S.; Potts, J. R.; Campbell, I. D.; Boyd, J. Probing protein-peptide binding surfaces using charged stable free radicals and transverse paramagnetic relaxation enhancement (PRE). *J. Biomol. NMR* **2005**, *31* (2), 155–160.
(17) Jahnke, W. Spin labels as a tool to identify and characterize protein−ligand interactions by NMR spectroscopy. *ChemBioChem* **2002**, *3* (2−3), 167–173.
(18) Vazquez, J.; De, S. K.; Chen, L.-H.; Riel-Mehan, M.; Emdadi, A.; Cellitti, J.; Stebbins, J. L.; Rega, M. F.; Pellecchia, M. Development of paramagnetic probes for molecular recognition studies in protein kinases. *J. Med. Chem.* **2008**, *51* (12), 3460–3465.
(19) Marsilje, T. H.; Milkiewicz, K. L.; Hangauer, D. G. The design, synthesis and activity of non-ATP competitive inhibitors of pp60c-src tyrosine kinase. Part 1. Hydroxynaphthalene derivatives. *Bioorg. Med. Chem. Lett.* **2000**, *10* (5), 477–481.
(20) Milkiewicz, K. L.; Marsilje, T. H.; Woodworth, R. P., Jr.; Bifulco, N., Jr.; Hangauer, M. J.; Hangauer, D. G. The design, synthesis and activity of non-ATP competitive inhibitors of pp60c-src tyrosine kinase. Part 2. Hydroxyindole derivatives. *Bioorg. Med. Chem. Lett.* **2000**, *10* (5), 483–486.
(21) Hangauer, D. G. The Discovery of KX01: A Highly Selective, Non-ATP Competitive, Src Inhibitor. CHI's 5th Annual Protein Kinase Targets Meeting, Boston, June 4−6, 2007.
(22) Sofan, M. A.-M.; Abdel-Aziz El-Taweel, F. M.; El-Maati, T. A.; Ali El-Agamey, A.-G. Acylation reactions of 5-amino-3-phenylpyrazole: Routes to pyrazolopyrimidines, pyrazolodiazepine, pyrazoloquinazoline and pyrazolopyrrolopyrimidine derivatives. *Indian J. Chem., Sect. B: Org. Chem. Incl. Med. Chem.* **1994**, *33B* (8), 738–741.
(23) Elmaati, T. M. A.; El-Taweel, F. M. New trends in the chemistry of 5-aminopyrazoles. *J. Heterocycl. Chem.* **2004**, *41* (2), 109–134.
(24) Gavrin, L. K.; Lee, A.; Provencher, B. A.; Massefski, W. W.; Huhn, S. D.; Ciszewski, G. M.; Cole, D. C.; McKew, J. C. Synthesis of pyrazolo[1,5-α]pyrimidinone regioisomers. *J. Org. Chem.* **2007**, *72* (3), 1043–1046.
(25) Springer, R. H.; Scholten, M. B.; O'Brien, D. E.; Novinson, T.; Miller, J. P.; Robins, R. K. Synthesis and enzymic activity of 6-carbethoxy- and 6-ethoxy-3,7-disubstituted pyrazolo[1,5-a]-pyrimidines and related derivatives as adenosine cyclic 3′,5′-phosphate phosphodiesterase inhibitors. *J. Med. Chem.* **1982**, *25* (3), 235–242.
(26) Anwar, H. F.; Elnagdi, M. H. Recent developments in aminopyrazole chemistry. *ARKIVOC* **2009**, *1*, 198–250.

(27) Juffermans, J. P. H.; Habraken, C. L. Pyrazoles. 19. Selective thermolysis reactions of bromo-1-nitro-1H-pyrazoles. Formation of 3-nitro-1H- vs. 4-nitro-1H-pyrazoles. *J. Org. Chem.* **1986**, *51* (24), 4656–4660.
(28) Lepre, C. A.; Moore, J. M.; Peng, J. W. Theory and applications of NMR-based screening in pharmaceutical research. *Chem. Rev.* **2004**, *104* (8), 3641–3675.
(29) Mayer, M.; Meyer, B. Characterization of ligand binding by saturation transfer difference NMR spectroscopy. *Angew. Chem., Int. Ed.* **1999**, *38* (12), 1784–1788.
(30) Berger, S. *200 and More NMR Experiments*; Wiley-VCH: Weinheim, Germany, 2004.
(31) Leipert, T. K.; Noggle, J. H.; Freeman, W. J.; Dalrymple, D. L. Rotating frame nuclear relaxation of PBr_3: Off-resonance studies by Fourier transform NMR. *J. Magn. Reson.* **1975**, *19*, 208–221.
(32) Bemis, G. W.; Murcko, M. A. The properties of known drugs. 1. Molecular frameworks. *J. Med. Chem.* **1996**, *39* (15), 2887–2893.
(33) Hangauer, D. G. Biaryl compositions and methods for modulating a kinase cascade, preparation, pharmaceutical compositions, and use in the treatment of diseases. US 2007/0015752 A1, 2007.
(34) Dalgarno, D.; Stehle, T.; Narula, S.; Schelling, P.; van Schravendijk, M. R.; Adams, S.; Andrade, L.; Keats, J.; Ram, M.; Jin, L.; Grossman, T.; MacNeil, I.; Metcalf, C., III; Shakespeare, W.; Wang, Y.; Keenan, T.; Sundaramoorthi, R.; Bohacek, R.; Weigele, M.; Sawyer, T. Structural basis of Src tyrosine kinase inhibition with a new class of potent and selective trisubstituted purine-based compounds. *Chem. Biol. Drug Des.* **2006**, *67*, 46–57.
(35) Emsley, L.; Bodenhausen, G. Gaussian pulse cascades: New analytical functions for rectangular selective inversion and in-phase excitation in NMR. *Chem. Phys. Lett.* **1990**, *165* (6), 469–476.
(36) Ernst, R. R.; Bodenhausen, G.; Wokaun, A. *Principles of Nuclear Magnetic Resonance in One and Two Dimensions*; Clarendon Press: Oxford, U.K., 1987; Vol. 14.
(37) Otwinowski, Z.; Minor, W. Processing of X-ray diffraction data collected in oscillation mode. *Methods Enzymol.* **1997**, *276*, 307–326.
(38) Emsley, P.; Cowtan., K. Coot: Model-building tools for molecular graphics. *Acta Crystallogr.* **2004**, *D60*, 2126–2132.
(39) Adams, P. D.; Gopal, K.; Grosse-Kunstleve, R. W.; Hung, L.-W.; Ioerger, T. R.; McCoy, A. J.; Moriarty, N. W.; Pai, R. K.; Read, R. J.; Romo, T. D.; Sacchettini, J. C.; Sauter, N. K.; Storoni, L. C.; Terwilliger, T. C. Recent developments in the PHENIX software for automated crystallographic structure determination. *J. Synchrotron Radiat.* **2004**, *11*, 53–55.